Heliyon 10 (2024) e40547

Contents lists available at ScienceDirect

Heliyon

journal homepage: www.cell.com/heliyon

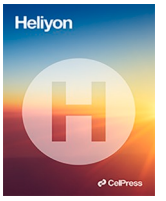

Research article

A novel nature-inspired ligno-alginate hydrogel coated with Fe_3O_4/GO for the efficient-sustained release of levodopa

Athira K [a], B Siva Kumar [a,*], S Giridhar Reddy [a], K. Prashanthi [b], Sanga Kugabalasooriar [c], Jyothi Kumari Posa [d]

[a] Department of Physical Sciences, Amrita School of Engineering, Bengaluru, Amrita Vishwa Vidyapeetham, 560035, India
[b] Department of Biotechnology, Ramaiah University of Applied Sciences, Bengaluru, 560054, India
[c] Department of Chemistry, Northeastern University, Boston, MA, 02115, United States
[d] Department of Biosciences, Sri Sathya Sai Institute of Higher Learning, Anantapur, Andhra Pradesh, 515001, India

ARTICLE INFO

Keywords:
Sodium alginate
Levodopa
Graphene oxide
Drug release
Parkinson's disease

ABSTRACT

Levodopa (LD), a precursor to dopamine, is commonly used to treat Parkinson's disease. However, its oral formulations suffer from low bioavailability, toxicity, and untargeted delivery. This study aimed to develop a nature-based hydrogel for sustained LD release, addressing these limitations. The hydrogel was synthesized using sodium alginate (SAl) and lignosulfonic acid (LSA) as polymers, cross-linked with Ba^{2+} ions, and coated with iron oxide nanoparticles (Fe_3O_4) and graphene oxide nanoparticles (GO). The resulting ligno-alginate films were characterized by Fourier Transform Infrared Spectroscopy (FTIR), X-ray Diffraction (XRD), Thermogravimetric Analysis (TGA), and Field Emission Scanning Electron Microscopy (FESEM). *In-vitro* drug release was evaluated using UV–visible spectroscopy. The formulations LD 2 (SAl-LSA-GO-LD) and LD 3 (SAl-LSA-Fe_3O_4-GO-LD) demonstrated superior sustained release properties, attributed to the hydrophobic layer provided by GO, which controlled the swelling rate and slowed drug diffusion. LD 2 showed the highest drug loading efficiency at 69 % and a sustained release of 24 % over 48 h, which was better than previously reported work of 64 % in 30 h. Incorporating Fe_3O_4 endowed the delivery vehicle with magnetic properties for targeted drug delivery. This study presents a novel and efficient approach for the sustained release of LD using a ligno-alginate hydrogel coated with Fe_3O_4 and GO, offering promising potential for Parkinson's treatment.

1. Introduction

Parkinson's disease (PD) is a neurological condition characterized by the degeneration of nerve cells in the central nervous system, leading to significant motor and non-motor symptoms [1]. Levodopa (L-3,4-Dihydroxyphenylalanine), a precursor to dopamine, is a standard treatment; however, its oral formulations exhibit low bioavailability, toxicity, and untargeted delivery [2,3]. This paper explores a novel ligno-alginate hydrogel system enhanced with Fe_3O_4 and graphene oxide (GO) to address these challenges, focusing on controlled and sustained release.

The current therapeutic approaches for PD highlight the necessity for specific drug delivery systems that can enhance bioavailability while minimizing side effects. Controlled drug delivery systems facilitate a regulated and sustained release, improving patient

* Corresponding author.
E-mail address: b_sivakumar@blr.amrita.edu (B.S. Kumar).

https://doi.org/10.1016/j.heliyon.2024.e40547
Received 14 May 2024; Received in revised form 26 September 2024; Accepted 18 November 2024
Available online 19 November 2024

compliance [4]. These systems can be further augmented by integrating stimuli-responsive conditions (pH, heat, magnetic force) to achieve targeted drug release [5]. Recent studies have demonstrated innovative drug delivery systems for levodopa. Hao et al. in the year designed gastro-floating sustained-release capsules for levodopa and benserazide hydrochloride, achieving cumulative drug releases of 74 %, 85 %, and 95 % with different formulations [6]. Similarly, Nidhi et al. engineered a tricompartmental polymeric microcarrier for three PD drugs, reporting nearly 100 % encapsulation efficiency and complete drug release within 24 h [7]. Stalin Kondaveeti et al. developed magnetic-responsive hydrogels that utilized magnetic stimulation for prolonged levodopa release for about 30 h [8]. These advancements emphasize the critical need for therapies that mitigate the issues of low bioavailability and rapid degradation while ensuring sustained drug release for improved patient outcomes.

Considering the challenges, this study proposes a ligno-alginate hydrogel to improve sustained release profiles. The hydrogel incorporates Fe_3O_4 and GO, crosslinked with Ba^{2+} ions. Alginate, a biocompatible polysaccharide sourced from brown seaweed, is favored for its gel-forming ability and non-toxicity [9,10]. Alginate becomes water-soluble upon treatment with a basic solution, forming gels through ionic interactions with divalent and trivalent cations [11,12]. Lignin, a biodegradable polymer, offers additional benefits, such as antimicrobial properties and the ability to regulate the release of both hydrophobic and hydrophilic compounds [13,14]. Lignosulfonic acid, derived from the pulping process, maintains amphiphilic characteristics that enhance drug diffusion through hydrogel cross-linking [15,], [16]. The swelling capacity of lignin can be adjusted to optimize drug release rates, as evidenced by studies demonstrating that hydrogen bonding between lignin and other polymers affects their viscoelastic behaviour [17]. Furthermore, stimuli-sensitive hydrogels can optimize drug targeting and efficacy by responding to changes in pH and temperature [18–21].

Aashli et al. fabricated a transdermal film using sodium alginate and lignosulphonic acid (LSA) as a polymer matrix, achieving controlled drug release for montelukast sodium over 36 h [22]. Fe_3O_4 nanoparticles are renowned for their biocompatibility and magnetic properties, which can enhance targeted drug delivery when functionalized with polymers and GO [23]. Bahaar et al. demonstrated a sustained release system using magnetic nanoparticles coated with LSA and polyethylene glycol, achieving controlled drug release profiles [24]. Moreover, GO's large surface area and functional groups enable effective drug loading, enhancing the controlled release properties of various drug delivery systems [25–27]. Rashedi et al. created a biocompatible hydrogel combining chitosan, agarose, and GO, leading to improved drug loading and sustained release profiles for 5-fluorouracil [28].

The combination of sodium alginate, LSA, GO, and Fe_3O_4 presents a promising approach for sustained drug delivery. The novelty of this work lies in the synergistic effects of these materials, which collectively improve drug encapsulation and release profiles. Developing a hydrogel using an alginate-LSA film with Fe_3O_4 and GO could yield promising results for the sustained release of levodopa, addressing critical challenges in Parkinson's disease treatment.

2. Materials and methods

2.1. Materials

SAl (MW = 216.12 g/mol) and LSA (MW = 490.5 g/mol) were obtained from Sigma Aldrich, and ferric chloride [$FeCl_3.6H_2O$] (MW = 270.295 gm/mol) and ferrous sulfate anhydrous [$FeSO_4$] (MW = 151.91 g/mol) were obtained from Loba Chemicals. Barium chloride (MW = 208.23 g/mol) was obtained from S.D. Fine Chem. Ltd. Ammonium solution (NH_4OH) (MW = 17.031 g/mol) and graphene oxide (MW = 2043.8 g/mol) were obtained from Thermofisher Scientific Ltd. Levodopa was obtained as a pharmaceutical sample.

2.2. Synthesis of hydrogels

2.2.1. SAl and LSA blends

2 % SAl and LSA films were prepared at a ratio of 80:20 procedure adapted from a previously reported work [29]. The polymer was dissolved in distilled water via a magnetic stirrer for 30 min to obtain a uniform distribution. The blended mixture was subsequently poured onto a glass Petri plate and dried in a hot air oven at 45 °C for 16–24 h. The dried polymeric gel was cross-linked in 2 % barium chloride for 15 min to strengthen the polymeric interactions, and the films were subsequently dried at room temperature. The films were weighed and cut into 300 mg portions for surface coating(refer to the supplementary file for figures).

2.2.2. SAl-LSA-GO

Approximately 22 mg of GO was ultrasonicated at room temperature for 2 h r in 50 ml of distilled water to obtain a uniform dispersion. Then, the crosslinked dried SAl-LSA polymeric films were immersed in the GO solution and ultrasonicated for 1 h.

2.2.3. SAl-LSA-Fe_3O_4-GO

Synthesis of Fe_3O_4 and GO Solution: Approximately 1 g of $FeCl_3.6H_2O$ and 0.4 g of $FeSO_4$ were weighed and dissolved in 50 ml of distilled water, and the solution was stirred on a magnetic stirrer for 15 min at 60 °C. Then, ammonia solution was added dropwise to precipitate the Fe_3O_4 nanoparticles. The iron oxide nanoparticles were filtered out and dried. The Fe_3O_4 powder was dispersed in 25 ml of distilled water and added dropwise into 50 ml of GO solution (400 μg/ml); the solution was sonicated for 2 h.

The polymeric films were sonicated for 1 h in the Fe_3O_4-GO solution. The resulting SAl-LSA film coated with Fe_3O_4-GO was removed and dried at room temperature.

2.3. Loading of LDs into hydrogels

The process for loading LDs into polymeric films is described below. First, the dried polymeric films were fully submerged in 50 mL of freshly prepared LD solution (1 mg/ml).

The samples were then left to soak for 12 h at a temperature of 4 °C and protected from light during this time. This is necessary to avoid any light-induced degradation of the drug (refer to the supplementary file for figures).

2.4. Characterization

The FTIR spectra of the different formulations at different stages were investigated for the presence of the drug encapsulated in the polymer as well as the presence of unique functional groups in the nanoparticles. The FTIR instrument (Shimadzu, Model no. 206-31000-58, IR Spirit-L) was calibrated via potassium bromide KBr pellets by running the background scan. The drug release profiles of the polymers were evaluated at 280 nm via a UV–visible spectrophotometer (Shimadzu 2600).

Thermal characteristics such as the change in weight as a function of temperature up to 1500 °C (Thermogravimetric analysis (TGA) and differential scanning calorimetry (DSC)) were determined via a thermogravimetric analyzer (TA, USA-SDT Q600).

The crystallinity of the powdered materials was examined via XRD with a Rigaku Japan Ultima IV instrument. The signals are generated because of microstructure and phase transitions. A diffraction angle of 5°–90° was used to determine the crystal structure and intermolecular distances of the samples.

2.5. In vitro levodopa release studies

The release of LD was studied *in vitro* via a UV–vis spectrophotometer by immersing the film in 10 mL of buffer solution at pH 7.4. The calibration curve for the spectrophotometric analysis is included in the supplementary material. At every 2-h interval, 2 mL of the buffer solution was removed and analyzed via spectrophotometry at 280 nm [30].

$$\text{Release } (\%) = \frac{M_t}{M_i} \times 100 \qquad \text{Eq. (A.1)}$$

where M_t and M_i are the concentrations of drug released at time t and the initial loaded drug content, respectively.

2.6. Release kinetics of levodopa from polymeric films

Multiple mechanical release patterns for polymer formulations have been proposed under *in vitro* circumstances via standard mathematical kinetic models. The tested models comprised zero-order, first-order, Korsmeyer-Peppas, Higuchi, Kopcha, and Sahlins-Peppas models.

Zero-order drug release is the process of releasing a drug from a carrier at a constant rate independent of the initial drug concentration.

First-order drug release kinetics describe how the rate of drug release from a delivery system is proportional to the amount of drug present in the device at any given point in time. The amount of drug released decreases over time as the concentration gradient decreases. The release exponent, n, is derived from the Korsmeyer–Peppas model. At $n = 0.43$, drug release is described as Fickian diffusion, with no significant deformation or strain. Quasi-Fickian diffusion occurs when $n < 0.43$. When n is less than 0.85, drug release occurs through anomalous diffusion, which might cause swelling or stress due to variations in temperature, activity, or structural dimensions. If n exceeds 0.85, Case II transport occurs.

The Kopcha model was used to quantify the impact of diffusion and erosion on release patterns. The constants A = diffusion and B = erosion was used to determine which factor had a greater mathematical impact on release. The literature suggests that when A/B = 1, diffusion and erosion are equal. When A/B is less than 1, erosion takes precedence over diffusion, whereas when A/B is greater than 1, diffusion is dominant.

The Higuchi model is a mathematical model for calculating drug release from colloidal nanoparticles. The model uses Fickian diffusion to characterize drug release from an insoluble matrix as a square root of a time-dependent process.

In the Sahlin–Peppas model, when R/F equals one, the release mechanism includes both erosion and diffusion equally. When R/F is greater than one, relaxation (erosion) takes precedence over diffusion [31,32]. The formulas of these models are included in the supplementary file.

2.7. Biocompatibility of the ligno-alginate hydrogel

The Neuro-2A neuroblastoma cell line was procured from the National Centre for Cell Science, Pune, India. Neuro-2A cells were grown in T25 culture flasks containing Dulbecco's Modified Eagle Medium (DMEM) with 10 % Fetal Bovine Serum (FBS), along with 1 % of antibiotics, viz., penicillin 100 Units/ml and streptomycin 100 μg/ml. Cells were maintained in a humid atmosphere at 37 °C, containing 5 % carbon dioxide. Cell cytotoxicity was determined by the MTT method. For the cell cytotoxicity assay, cells (approximately 1×10^4 cells/well) were seeded into 96-well tissue culture plates, and 24 h after seeding, the medium was changed and cells were treated with various concentrations of pure Levodopa, SAl-LSA-GO-Fe_3O_4 (without LD) and SAl-LSA-GO-Fe_3O_4 -LD ranging from

0 to 100 μg (μg/ml) for 72 h. Cell viability was determined based on the principle that living cells will reduce the yellow-colored tetrazolium salt to a purple formazan product. This formazan product was dissolved in Dimethyl Sulfoxide (DMSO)and the absorbance was measured at 570 nm.

3. Results and discussion

3.1. Characterisation of the hydrogels

3.1.1. Fourier transform infrared studies

LD 1 FTIR spectra are shown in Fig. 1 d show the following absorbance peak at 1033 cm^{-1}, which represents C-O group elongation, and at 1419 cm^{-1}, which represents a symmetric stretching of COO, indicating the characteristic peaks of SAl-LSA [33] (Fig. 1 b). A characteristic peak of levodopa (Fig. 1e), Phenyl group C=C vibrations are present at 1450 cm^{-1} and 2938 cm^{-1}, representing carboxylic acid O-H stretching, which was originally found at 2978 cm^{-1} [34], showing a bathochromic shift due to the interaction of LDs with the polymer blend containing SAl-LSA.

The LD 2 spectra shown in Fig. 1a presents a peak at 1033 cm^{-1}, which represents C-O group elongation, and at 1619 cm^{-1}, which represents conjugated carbonyl stretching, indicating the presence of SAl-LSA. The peak at 1520 cm^{-1} represents C-OH bending, and the peak at 1062 cm^{-1} represents the vibration mode of C–O–H, indicating the presence of GO [35], and the LD characteristic peak observed at 2938 cm^{-1} represents carboxylic acid O–H stretching.

LD 3 FTIR spectra are shown in Fig. 1c Peak at 1033 cm^{-1} represents C-O group elongation and the peak at 1619 cm^{-1} represents conjugated carbonyl stretching, indicating the presence of SAl-LSA. The peak at 1520 cm^{-1} represents C-OH bending, indicating the presence of GO, the LD characteristic peak observed at 2938 cm^{-1} represents carboxylic acid O-H stretching, and the peak at 616 cm^{-1} is attributed to the Fe-O vibrational mode [36]. In the range of 1620–1650 cm^{-1}, the intensity of the peaks is elongated due to CO-groups from different components, indicating the presence and interaction of the polymer with the drug and nanoparticles.

3.1.2. X-ray diffraction

The XRD spectrum of SAl-LSA (Fig. 2b) revealed a peak at 13.5° due to the reflection of their plane from polyguluronate unit of SAl and broad haloes with the absence of Bragg reflections, indicating that the polymer was amorphous [37]. In the patterns of the drug-polymer composite LD 1 (Fig. 2e) and LD 2 (Fig. 2a), only a broad halo is detected without any distinctive peak of LD, confirming that the drug is present as an amorphous solid dispersion within the composite material.

The pure LD (Fig. 2c) appeared at 18.49° and 22.33°, indicating the crystalline structure of the drug [38]. The formulation LD 3 (Fig. 2d) is crystalline despite the polymer structure of the Fe_3O_4 particles, which enhances the crystalline nature of the composite at 30.73° and 42.92° [39].

The addition of crystalline materials to a drug delivery system leads to a more controlled and sustained drug release due to their slower dissolution rates. They enhance stability by protecting the drug against the environment and improve the mechanical strength and integrity of the system. Crystalline materials also allow modulation of the drug release rate and impact drug-polymer interactions, usually leading to slower release and sustained therapeutic effects [40].

Here the incorporation of crystalline materials like Fe_3O_4 and GO influence the nature of drug release which showed a sustained profile when compared to the hydrogel without the crystalline materials.

The crystal morphology of a material influences the dissolution rate of the drug because crucial elements, such as the surface area, size, and even the polymorphic form of the material, may affect the rate and extent of absorption.

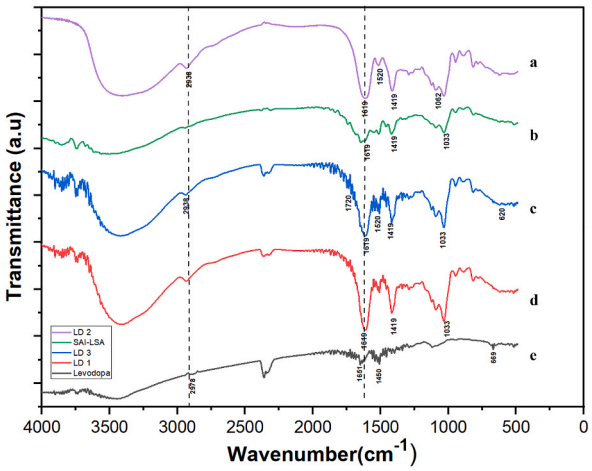

Fig. 1. FTIR spectra of **(a)** LD 2 **(b)** SAl-LSA **(c)** LD 3 **(d)** LD 1 **(e)** Levodopa.

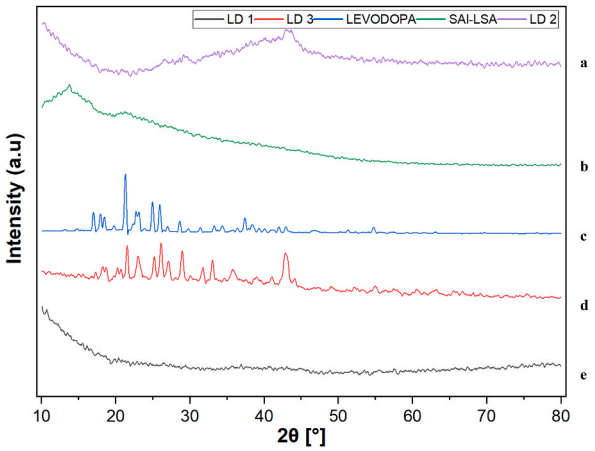

Fig. 2. XRD peaks of **(a)** LD 2 **(b)** SAl-LSA **(c)** Levodopa **(d)** LD 3 **(e)** LD 1.

3.1.3. Thermogravimetric analysis

The composition of a polymer, its degree of hydration, its thermal stability, and the amount of moisture or residual solvent can all be ascertained via TGA, as shown in Fig. 3. Heating from room temperature to 100 °C caused the first significant weight loss of approximately 10–12 %, which was attributed to the evaporation of trapped and physiosorbed water from the sample.

At temperatures greater than 100 °C, the structure of LSA and SAl (Fig. 3d) and weight loss show stages of degradation. The primary causes of the second weight loss of approximately 33–35 % in the range of 150–250 °C are attributed to carbon dioxide, carbon monoxide, and the evaporation of other pyrolysis products in lignin and the breakage of -OH bonds in SAl [41,42].

The breakdown of levodopa is caused by dihydroxylation in this temperature range. Furthermore, the loss of mass between 200 °C and 400 °C is attributed to the disintegration of hydroxyl groups, epoxy, and carboxyl oxygen-containing functional groups on the surface of the GO (Fig. 3b), compromising its quality at higher temperatures [43]. Fe_3O_4 (Fig. 3c), the nanoparticles are thermally stable throughout the process. These findings highlight the need to select appropriate surface coatings for the polymer to ensure its thermal stability.

3.1.4. Surface morphology

The surface morphology and shape of the magnetic nanoparticles were studied via FESEM, as shown in Fig. 4 a-d. The study used an EHT detector with a 10 kV accelerating voltage to investigate nanoparticle dispersion within the polymeric matrix. The FESEM micrograph revealed nearly spherical-shaped Fe_3O_4 nanoparticles with frequent agglomeration caused by the interactions of magnetic nanoparticles.

Aggregations are inescapable because of factors such as interparticle interactions and magnetic.

The SEM-EDX results are shown in Fig. 4 e and f, the atomic percentages of iron, oxygen, carbon, barium, and chlorine for SAl-LSA coated with Fe-GO are 3.8 %, 19.1 %, 33.2 %, 39.8 %, and 1.8 %, respectively.

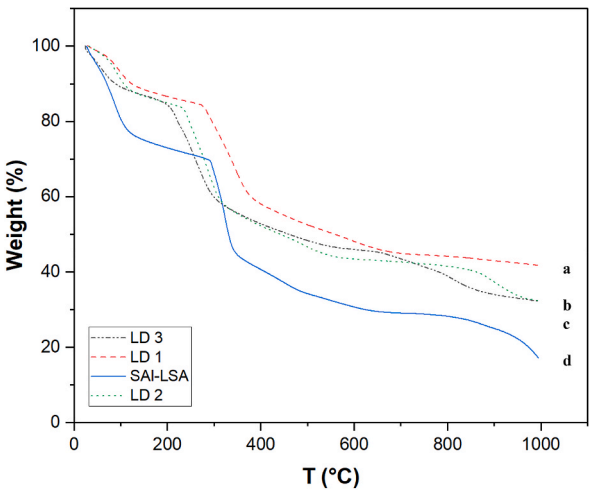

Fig. 3. TGA thermograms of **(a)** LD 1 **(b)** LD 2 **(c)** LD 3 **(d)** SAl-LS.

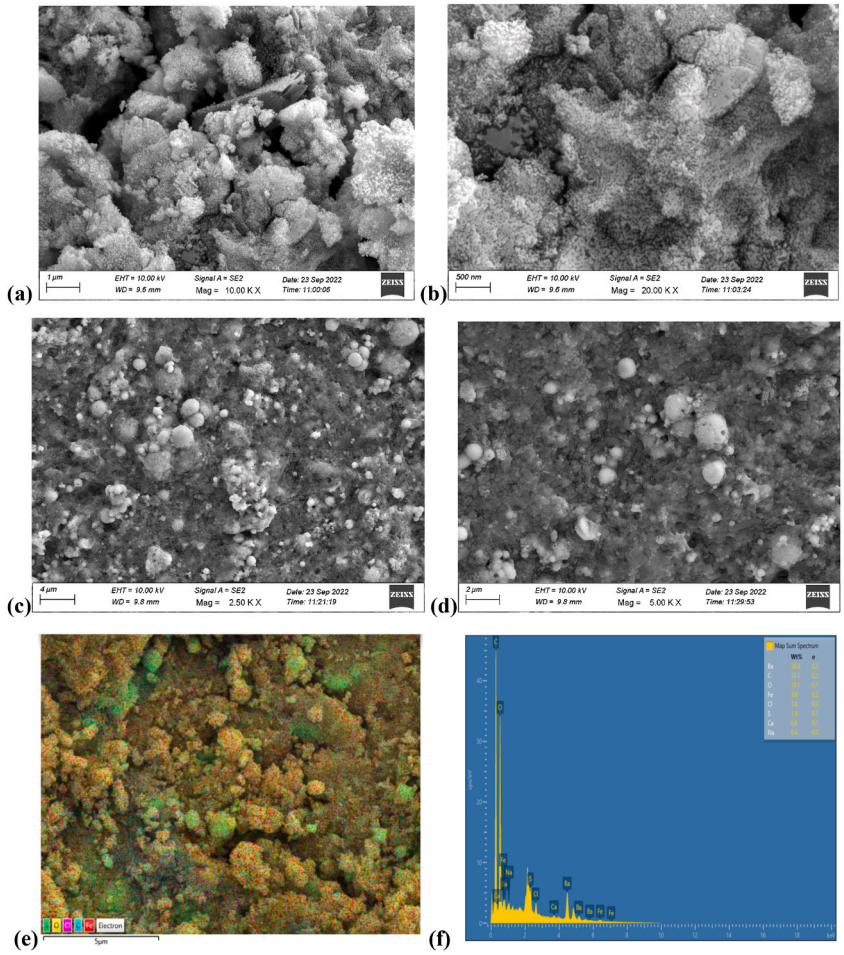

Fig. 4. FESEM images of LD 3 at different resolutions: **(a)** 1 μm**(b)** 500 nm **(c)** 4 μm **(d)** 2 μm **(e)** SEM-EDX layered image of LD 3 **(f)** SEM-EDX analysis of LD 3.

3.2. Loading efficiency and release profiles of LD

The loading efficiency of LDs on polymer-nanoform formulations was obtained by dissolving a known quantity of the drug by immersing the polymer film in the drug solution for 16 h. After 16 h, the film was removed, and the remaining solution was irradiated at 280 nm to calculate the concentration of free LD in the supernatant (C_t) by subtracting it from the initial LD concentration (C_0) and dividing it by C_0. The loading efficiency was expressed as a percentage via the following formula:

$$\text{Loading efficiency } (\%) = \frac{C_0 - C_t}{C_0} \times 100 \qquad \text{Eq. (A.2)}$$

The loading efficiency of LD was 68.41 %, 69.67 %, and 57.18 % in LD 1, LD 2, and LD 3 films, respectively, at pH 7.4. The loading efficiency of the films was better than that previously reported for 60 % loading efficiency [8]. In LD 1 and LD 2, the concentration of SAl is 80 % of the polymer matrix, which provides high drug loading capacity, as there are more polymer chains to encapsulate the drug. The inclusion of GO nanoparticles in the composition led to a slight increase in drug loading efficiency due to the larger surface area and the presence of a variety of oxygen-containing functional groups, including hydroxyl, epoxy, and carboxyl groups. These functional groups can interact with drug molecules through noncovalent interactions such as π−π stacking, hydrogen bonding, and electrostatic interactions. This allows for efficient drug loading onto the GO surface. Compared with that of the polymer matrix, the amount incorporated is small. In LD 3, incorporating Fe_3O_4 into drug delivery systems lowers drug loading through competitive binding, in which Fe ions compete with drug molecules for binding sites on the carrier material. In addition, Fe ions may cause the carrier material to aggregate, reducing the surface area accessible for drug adsorption. Chemical interactions between the Fe ions and functional groups of sodium alginate or graphene oxide may reduce the drug loading efficiency.

The release profile of the LD from LD 1 after 48 h is depicted in Fig. 5 a. In the first 2 h, an initial burst of 16 % was observed, which indicates the superiority of the novel polymer composite over previous methods in terms of the controlled release of the drug. The release percentage increased by approximately 20 % every 2 h during the initial 6 h, indicating faster release of levodopa from the SAl-

LSA film. A total of 78 % of the drug was released within 30 h. After 48 h, the release values decreased from 78 % to 50 %, indicating the occurrence of drug degradation. LD 1 shows the best fit with the Sahlins-Peppas Model ($R^2 = 0.99$), suggesting that the drug release mechanism is more complex, involving both diffusion and relaxation processes. Sahlins-Peppas is the most suitable model for LD 1 due to the high R2 showing a clear dominance of polymer relaxation and erosion.

Sodium alginate swells faster in a pH 7.4 environment because of the ionization of the carboxyl group. resulting in the creation of negatively charged carboxylate ions. This enhanced ionization increases the repulsive interactions between the negatively charged groups throughout the alginate chain, resulting in greater swelling.

The release profile of levodopa from LD 2 for 48 h is depicted in Fig. 5b. In the first 2 h, the release profile of levodopa from LD 2 was 12 %, which was less than that of LD 1. Approximately 24 % of the drug was released within 48 h, indicating that the controlled release of levodopa was much better than that of LD 1 and LD 3. The controlled release could be attributed to the amphiphilic nature of GO, which influences the release of LD from the films. The presence of GO with SAl can affect drug release kinetics by acting as a barrier, as it forms a hydrophobic layer, limiting drug diffusion.

The release profile of levodopa for LD 3 after 48 h is depicted in Fig. 5c. In the first 2 h, the release profile is 19 %. Approximately 28 % of the drug was released within 48 h, indicating that the controlled release of levodopa was much better than that of LD 1 but not as efficient as that of LD 2. The incorporation of Fe_3O_4 can enhance drug biological activity by achieving magnetically assisted targeted drugs. GO increases the drug loading capacity and enables sustained release of the drug. The magnetic nanoparticle-incorporated formulation paved the way for targeted drug delivery, indicating the efficiency of the novel hydrogel for controlled release applications in a sustained manner.

For both LD 2 and LD 3, the drug release is primarily diffusion-controlled, with the Korsmeyer-Peppas model showing the best fit with $R^2 = 0.97$ for LD 2, and $R^2 = 0.96$ for LD 3. This indicates that the release is governed by a combination of diffusion and relaxation mechanisms in both formulations.

A quantitative comparison of the existing biopolymeric system to encapsulate levodopa and the controlled release profile is summarized in Table 1.

Compared with previous literature as depicted in Table 1, the drug delivery performance of this study is significantly improved. In Hao et al. [6] and Nidhi et al. [7], though the drug release percentage was high, the duration for the release was relatively shorter up to 12 h and 24 h, respectively. Stalin Kondaveeti et al. [8] achieved a drug release time of 30 h with a lower drug load. In contrast, in magnetic-GO hydrogels with eco-friendly polymers—SAl and LSA—in our work, we observed a substantial drug load of about 57.14 %–69 %, coupled with a sustained release of 24 %–28 % for an extended period of 48 h. This extended period of the release with significant drug loading underlines better efficacy and stability of our hydrogels for controlled drug delivery applications.

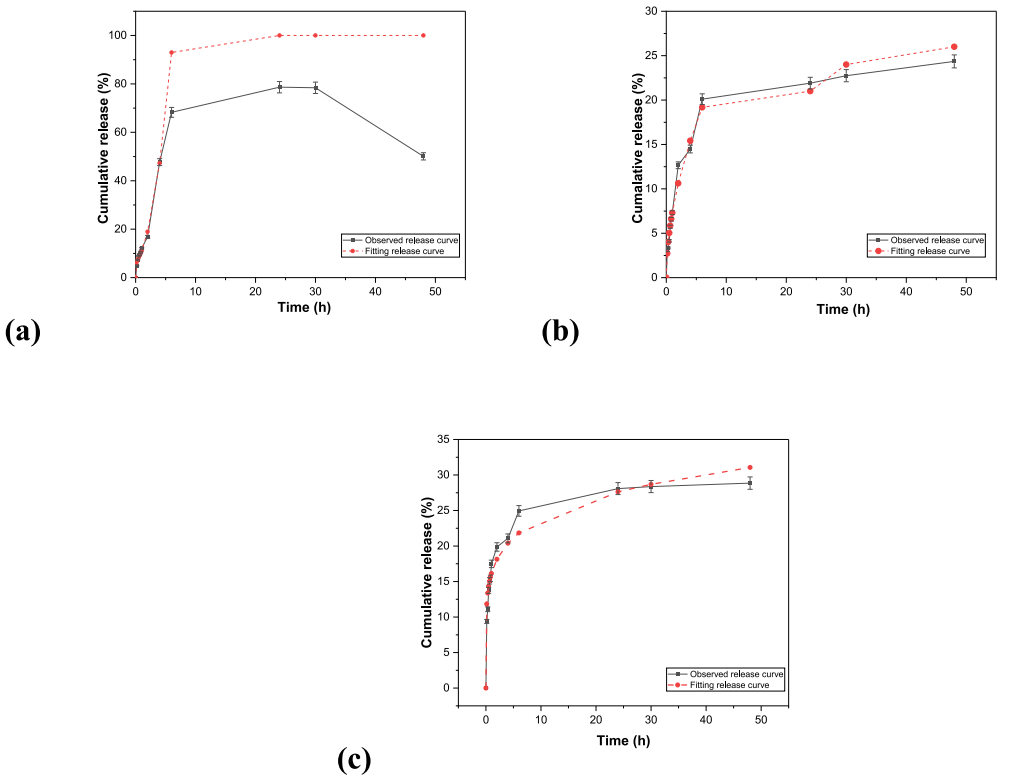

Fig. 5. Release profiles of **(a)** LD 1 **(b)** LD 2 **(c)** LD 3.

Table 1
Comparison of existing formulations with the current study.

Study	Formulation Details	Drug load/% Drug release/duration
Hao et al. [6]	Sodium dodecyl sulfate, polyethylene oxide, NaCl, and cellulose acetate	NA/SDS: 74 %, PEO N-80: 85 %, NaCl: 95 %/12 h
Nidhi et al. [7]	PLA (Polylactic Acid), PLGA (Poly (lactic-co-glycolic acid)), PCL (Polycaprolactone), and PEG (Polyethylene Glycol).	100 %/100 % release/24 h
Stalin Kondaveeti et al. [8]	Magnetic-responsive hydrogels of xanthan gum and sodium alginate, cross-linked with calcium chloride.	64 %/66 % release/30 h
Present Study	Magnetic-GO hydrogels prepared with eco-friendly polymers SAlg and LSA, for levodopa delivery.	LD 2: 69 %/24 % release/48 h LD 3: 57.14 %/28 % release/48 h

3.3. Drug release kinetics of LD

The zero-order rate constant (k_0) is greater in LD 1 than in LD 2 and LD 3, indicating that there is fast drug release, which remains constant over time.

The first-order kinetics show a high value of k of 1.12 in LD 1, indicating a faster release rate than in LD 2 and LD 3. In the Higuchi model, the k value in LD 1 is relatively high, indicating that the drug is released from the matrix system at a relatively fast rate, whereas LD 2 and LD 3 have relatively low k values, indicating a relatively slow release rate, as shown in Table 2.

In the Korsmeyer–Peppas model, as shown in Table 3 in LD 1, the n value was 0.94, indicating "super case II transport," which differs greatly from Fickian diffusion. This behavior points to a release mechanism based on polymer relaxation rather than drug diffusion. In LD 2, $n = 0.53$ indicates anomalous diffusion of the drug, whereas in LD 3, n is 0.16, which suggests a release mechanism similar to Fickian diffusion, indicating that drug release is mostly regulated by diffusion through the polymer matrix. This trend is typical in systems where drug release is predominantly controlled by molecular diffusion and adheres to classical diffusion principles.

In the Kopcha model of LD 1, B (erosion constant) is greater than A (diffusion constant), and the A/B ratio is less than 1, indicating that the erosion mechanism is predominant for drug release, whereas in LD 2 and LD 3, A (diffusion constant) is greater than B (erosion constant), and A/B is greater than 1, which shows that drug release is governed by diffusion.

In the Peppas model, the R/F ratio in LD 1 is greater than 1, indicating that the relaxational mechanism is the dominant phenomenon governing the release of the drug, whereas in LD 2 and LD 3, the R/F ratio is less than 1, indicating that the diffusion mechanism is predominant, as shown in Table 2.

Based on the above discussion, the polymer-nanocomposite with GO and Fe_3O_4 follows a diffusion model, which is suitable for the drug release mechanism.

3.4. MTT assay-cell viability study

The MTT assay [3-(4,5-dimethylthiazol-2-yl)-2,5-diphenyltetrazolium) was used to assess the cytotoxicity of ligno-alginate containing levodopa on NeuroA2 cells, an established *in vitro* model for Parkinson's disease due to its neuronal characteristics. The study compared the effects of polymer vehicle SAl-LSA-Fe-GO without drug and SAl-LSA-Fe-GO-LD delivery systems, with levodopa, against NueroA2. The results indicated that cell viability, for all formulations, was dependent on the dose and time, varied in their cytotoxicity, and effectiveness in the setting of neuroprotection and drug delivery. As expected, the Levodopa-induced cell death is clear as seen in Fig. 6 (a) (Orange bar in the graph). In contrast, the ligno-alginate nanocomposite vehicle shown in Fig. 6 (a) (the purple bar) without the drug demonstrated negligible effects on cell viability showing the biocompatibility nature of the ligno-alginate hydrogel. The reduced cell viability for SA-LSA-Fe-GO-LD shown in Fig. 6 (a) (the green bar) treated cells is attributed to the slow release of levodopa from the carrier. SA-LSA-Fe-GO and SA-LSA-Fe-GO-LD showed less toxicity and, therefore, were likely to exert a safer profile for such materials in drug delivery applications.

4. Conclusion

The findings of this study highlight that magnetic-GO hydrogels, developed using eco-friendly polymers SAl and LSA, create an excellent platform for drug delivery. The results indicate that LD 2 and LD 3 are promising candidates for formulating delayed and sustained-release medications for treating Parkinson's disease.

However, the study does encounter some limitations, such as the role of LSA as a binding agent in drug delivery, which restricts

Table 2
Release kinetics values for Zero, First, and Higuchi.

Model	Zero-order		First-order		Higuchi	
	k	R^2	k	R^2	k	R^2
LD 1	10.59	0.955	1.12	0.97	24.997	0.8649
LD 2	3.15	0.8847	0.54	0.83	8.1	0.95
LD 3	2.69	0.71	0.33	0.67	7.3	0.87

Table 3
Release kinetics values for Kopcha, Sahlins-Peppas and Kormeyer-Peppas.

Model	Kopcha			Sahlins-Peppas					Korsmeyer Peppas		
	A	B	R^2	K_d	K_r	m	R/F	R^2	k	N	R^2
LD 1	2.76	9.82	0.97	8.74	11.6	0.19	1.28	0.99	12.21	0.94	0.97
LD 2	7.03	0.30	0.97	7.21	0.1	0.512	0.01	0.97	7.31	0.53	0.97
LD 3	14.12	0.1	0.93	15.96	0.1	0.23	0.00	0.96	16.13	0.16	0.96

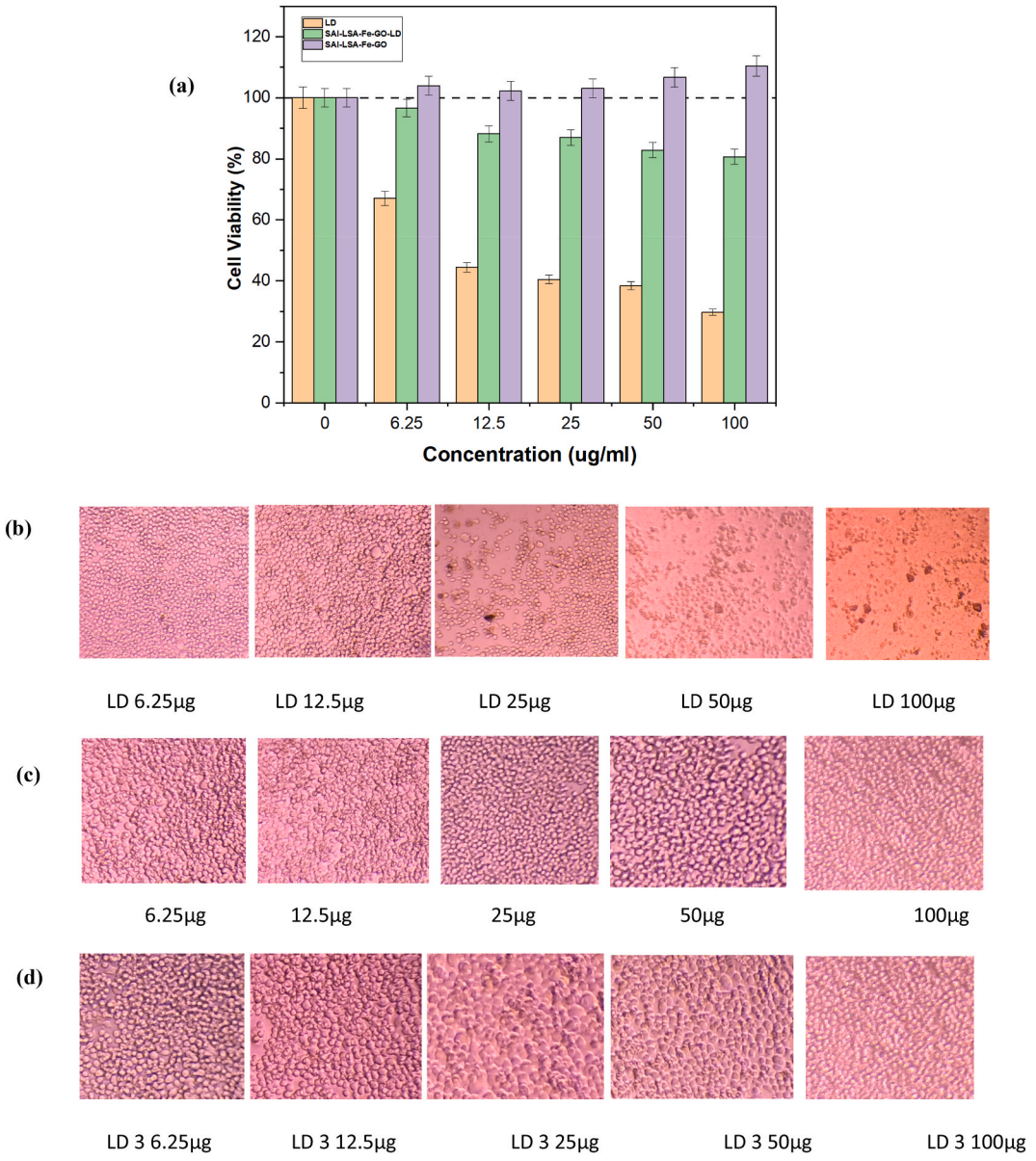

Fig. 6. **(a)** MTT assay cell proliferation of hydrogels at 72 h. **(b)** morphological appearance at 72 h for LD **(c)** morphological appearance at 72 h for SAl-LSA-Fe-GO **(d)** morphological appearance at 72 h for SAl-LSA-Fe-GO-LD.

comprehensive insights. Additionally, the absence of *in vivo* data hampers the validation of the formulation's efficacy and safety.

This study proposes a novel method for customizing and creating biocompatible magnetic materials capable of effectively releasing LD, potentially benefiting Parkinson's disease treatment. Specifically, LD 2 exhibited the highest drug loading efficiency at 69 % with a sustained release of 24 % over 48 h, while LD 3 demonstrated a drug loading efficiency of 57.14 % and a sustained release of 28 %.

Moreover, the integration of LSA with SAl represents a novel formulation that significantly enhances biocompatibility, controlled release characteristics, and mechanical strength. The addition of GO and Fe_3O_4 synergistically modifies the properties of the polymer components, showcasing the potential for developing innovative drug delivery systems for LD. This approach may improve therapeutic efficacy and reduce side effects, ultimately leading to better patient outcomes across various biomedical applications.

The formulation developed in this study aims to provide controlled drug release during medical procedures, ensuring sustained and accurate therapeutic effects at the target site. By maintaining optimal drug levels, controlled release mechanisms can enhance treatment efficacy and reduce the need for frequent dosing. The promising results from this formulation pave the way for further development and validation through *in vivo* clinical trials.

CRediT authorship contribution statement

Athira K: Writing – original draft, Methodology, Investigation, Formal analysis, Data curation. **B Siva Kumar:** Writing – review & editing, Validation, Supervision, Investigation, Data curation, Conceptualization. **S Giridhar Reddy:** Writing – review & editing, Validation, Supervision, Methodology, Investigation, Formal analysis, Data curation, Conceptualization. **K. Prashanthi:** Validation, Supervision, Resources. **Sanga Kugabalasooriar:** Writing – review & editing, Validation, Resources. **Jyothi Kumari Posa:** Validation, Data curation.

Availability of data and materials

The datasets used and/or analyzed during the current study are available from the corresponding author upon reasonable request.

Data availability statement

Data included in article/supp. material/referenced in the article.

Additional information

No additional information is available for this paper.

Funding

No funding available.

Declaration of competing interest

The authors declare that they have no known competing financial interests or personal relationships that could have appeared to influence the work reported in this paper.

Acknowledgments

We thank Amrita School of engineering, Amrita Vishwa Vidyapeetham, Bengaluru for all the facilities. We thank the Central Research Institute Facilities from Sri Sathya Sai Institute of Higher Learning, Puttaparthy, and Anantapur India, for TGA, SEM characterization, and cytotoxicity studies. We thank the COE-AMGT instrumentation facility from Amrita Vishwa Vidyapeetham, Coimbatore campus, for FESEM characterization. We sincerely thank all the individuals and organizations who supported us in completing this manuscript.

Appendix A. Supplementary data

Supplementary data to this article can be found online at https://doi.org/10.1016/j.heliyon.2024.e40547.

References

[1] D.M. Radhakrishnan, V. Goyal, 'Parkinson's disease, A review (2018), https://doi.org/10.4103/0028-3886.226451.
[2] T. Wang, et al., Highly efficient electrocatalytic oxidation of levodopa as a Parkinson therapeutic drug based on modified screen-printed electrode, Heliyon 10 (14) (Jul. 2024) e34689, https://doi.org/10.1016/j.heliyon.2024.e34689.
[3] J.G. Nutt, Pharmacokinetics and pharmacodynamics of levodopa, Movement Disorders 23 (S3) (2008) S580–S584, https://doi.org/10.1002/mds.22037.
[4] S. Adepu, S. Ramakrishna, Controlled drug delivery systems: current status and future directions, Molecules 26 (19) (Sep. 2021) 5905, https://doi.org/10.3390/molecules26195905.
[5] M.A. Rahim, et al., Recent advancements in stimuli responsive drug delivery platforms for active and passive cancer targeting, Cancers 13 (4) (2021) 670, https://doi.org/10.3390/cancers13040670. Feb.

[6] H. Yuan, Z. Zhang, L. Hu, Development and characterization of gastro-floating sustained-release capsule with improved bioavailability of levodopa, Drug Deliv Transl Res 13 (1) (Jan. 2023) 9–17, https://doi.org/10.1007/s13346-022-01188-5.

[7] N. Gupta, P.K. Sharma, S.S. Yadav, M. Chauhan, A.K. Datusalia, S. Saha, Tricompartmental microcarriers with controlled release for efficient management of Parkinson's disease, ACS Biomater. Sci. Eng. (Jul. 2024), https://doi.org/10.1021/acsbiomaterials.4c01042.

[8] S. Kondaveeti, A.T.S. Semeano, D.R. Cornejo, H. Ulrich, D.F.S. Petri, Magnetic hydrogels for levodopa release and cell stimulation triggered by external magnetic field, Colloids Surf. B Biointerfaces 167 (Jul. 2018) 415–424, https://doi.org/10.1016/j.colsurfb.2018.04.040.

[9] S. Giridhar Reddy, Alginates - a seaweed product: its properties and applications, in: Properties and Applications of Alginates, IntechOpen, 2022, https://doi.org/10.5772/intechopen.98831.

[10] N. Kavitha, et al., Formulation of alginate based hydrogel from brown seaweed, Turbinaria conoides for biomedical applications, Heliyon 5 (12) (Dec. 2019) e02916, https://doi.org/10.1016/j.heliyon.2019.e02916.

[11] D.M. Hariyadi, N. Islam, Current status of alginate in drug delivery, Adv Pharmacol Pharm Sci 2020 (Aug. 2020) 1–16, https://doi.org/10.1155/2020/8886095.

[12] S.G. Reddy, A.S. Pandit, Controlled drug delivery studies of biological macromolecules: sodium alginate and lignosulphonic acid films, J. Appl. Polym. Sci. 131 (13) (Jul. 2014), https://doi.org/10.1002/app.40442.

[13] J. Ruwoldt, A critical review of the physicochemical properties of lignosulfonates: chemical structure and behavior in aqueous solution, at surfaces and interfaces, Surfaces 3 (4) (Nov. 2020) 622–648, https://doi.org/10.3390/surfaces3040042.

[14] R. Kumar, et al., Lignin: drug/gene delivery and tissue engineering applications, Int J Nanomedicine 16 (Mar. 2021) 2419–2441, https://doi.org/10.2147/IJN.S303462.

[15] W. Chen, X. Peng, L. Zhong, Y. Li, R. Sun, Lignosulfonic acid: a renewable and effective biomass-based catalyst for multicomponent reactions, ACS Sustain Chem Eng 3 (7) (Jul. 2015) 1366–1373, https://doi.org/10.1021/acssuschemeng.5b00091.

[16] P. Karagoz, S. Khiawjan, M.P.C. Marques, S. Santzouk, T.D.H. Bugg, G.J. Lye, Pharmaceutical applications of lignin-derived chemicals and lignin-based materials: linking lignin source and processing with clinical indication, Biomass Convers Biorefin (Jan. 2023), https://doi.org/10.1007/s13399-023-03745-5.

[17] M. Culebras, A. Barrett, M. Pishnamazi, G.M. Walker, M.N. Collins, Wood-derived hydrogels as a platform for drug-release systems, ACS Sustain Chem Eng 9 (6) (Feb. 2021) 2515–2522, https://doi.org/10.1021/acssuschemeng.0c08022.

[18] N. Gull, et al., Designing of biocompatible and biodegradable chitosan based crosslinked hydrogel for in vitro release of encapsulated povidone-iodine: a clinical translation, Int. J. Biol. Macromol. 164 (Dec. 2020) 4370–4380, https://doi.org/10.1016/j.ijbiomac.2020.09.031.

[19] N. Gull, et al., Inflammation targeted chitosan-based hydrogel for controlled release of diclofenac sodium, Int. J. Biol. Macromol. 162 (Nov. 2020) 175–187, https://doi.org/10.1016/j.ijbiomac.2020.06.133.

[20] N. Gull, et al., *In vitro* study of chitosan-based multi-responsive hydrogels as drug release vehicles: a preclinical study, RSC Adv. 9 (53) (2019) 31078–31091, https://doi.org/10.1039/C9RA05025F.

[21] N. Gull, et al., Hybrid cross-linked hydrogels as a technology platform for *in vitro* release of cephradine, Polym. Adv. Technol. 30 (9) (Sep. 2019) 2414–2424, https://doi.org/10.1002/pat.4688.

[22] Aashli, S.G. Reddy, B. Siva Kumar, K. Prashanthi, H.C.A. Murthy, Fabricating transdermal film formulations of montelukast sodium with improved chemical stability and extended drug release, Heliyon 9 (3) (Mar. 2023) e14469, https://doi.org/10.1016/j.heliyon.2023.e14469.

[23] L. Shen, B. Li, Y. Qiao, Fe3O4 nanoparticles in targeted drug/gene delivery systems, Materials 11 (2) (Feb. 2018) 324, https://doi.org/10.3390/ma11020324.

[24] H. Bahaar, S.G. Reddy, B.S. kumar, P. K, M.H.C. A, Modified layered double hydroxide – PEG magneto-sensitive hydrogels with suitable ligno-alginate green polymer composite for prolonged drug delivery applications, Engineered Science (2023), https://doi.org/10.30919/es914.

[25] M. Hoseini-Ghahfarokhi, et al., ' Applications of graphene and graphene oxide in smart drug/gene delivery: is the world still flat? ', Int J Nanomedicine 15 (Nov. 2020) 9469–9496, https://doi.org/10.2147/IJN.S265876.

[26] A.M. Valencia, C.H. Valencia, F. Zuluaga, C.D. Grande-Tovar, Synthesis and fabrication of films including graphene oxide functionalized with chitosan for regenerative medicine applications, Heliyon 7 (5) (May 2021) e07058, https://doi.org/10.1016/j.heliyon.2021.e07058.

[27] B.M. Yoo, H.J. Shin, H.W. Yoon, H.B. Park, Graphene and graphene oxide and their uses in barrier polymers, J. Appl. Polym. Sci. 131 (1) (Jan. 2014), https://doi.org/10.1002/app.39628.

[28] M. Rajaei, H. Rashedi, F. Yazdian, M. Navaei-Nigjeh, A. Rahdar, A.M. Díez-Pascual, Chitosan/agarose/graphene oxide nanohydrogel as drug delivery system of 5-fluorouracil in breast cancer therapy, J. Drug Deliv. Sci. Technol. 82 (Apr. 2023) 104307, https://doi.org/10.1016/j.jddst.2023.104307.

[29] R.S. Giridhar, A.S. Pandit, Effect of curing agent on sodium alginate blends using barium chloride as crosslinking agent and study of swelling, thermal, and morphological properties, Int. J. Polym. Mater. 62 (14) (Jun. 2013) 743–748, https://doi.org/10.1080/00914037.2013.769236.

[30] Y. Ni, Y. Gu, S. Kokot, Simultaneous analysis of three catecholamines by a kinetic procedure: comparison of prediction performance of several different multivariate calibrations, Chem. Pap. 65 (6) (Jan. 2011), https://doi.org/10.2478/s11696-011-0090-6.

[31] F. Fischel-Ghodsian, J.M. Newton, Analysis of drug release kinetics from degradable polymeric devices, J. Drug Target. 1 (1) (Jan. 1993) 51–57, https://doi.org/10.3109/10611869308998764.

[32] Y. Fu, W.J. Kao, Drug release kinetics and transport mechanisms of non-degradable and degradable polymeric delivery systems, Expert Opin Drug Deliv 7 (4) (Apr. 2010) 429–444, https://doi.org/10.1517/17425241003602259.

[33] Q. Liu, Q. Li, S. Xu, Q. Zheng, X. Cao, Preparation and properties of 3D printed alginate–chitosan polyion complex hydrogels for tissue engineering, Polymers 10 (6) (Jun. 2018) 664, https://doi.org/10.3390/polym10060664.

[34] H. Bukhary, G.R. Williams, M. Orlu, Fabrication of electrospun levodopa-carbidopa fixed-dose combinations, Advanced Fiber Materials 2 (4) (Aug. 2020) 194–203, https://doi.org/10.1007/s42765-020-00031-1.

[35] T.F. Emiru, D.W. Ayele, Controlled synthesis, characterization and reduction of graphene oxide: a convenient method for large scale production, Egyptian Journal of Basic and Applied Sciences 4 (1) (Mar. 2017) 74–79, https://doi.org/10.1016/j.ejbas.2016.11.002.

[36] S.H. Chaki, T.J. Malek, M.D. Chaudhary, J.P. Tailor, M.P. Deshpande, Magnetite Fe $_3$ O $_4$ nanoparticles synthesis by wet chemical reduction and their characterization, Adv. Nat. Sci. Nanosci. Nanotechnol. 6 (3) (May 2015) 035009, https://doi.org/10.1088/2043-6262/6/3/035009.

[37] P. Sundarrajan, P. Eswaran, A. Marimuthu, L.B. Subhadra, P. Kannaiyan, One pot synthesis and characterization of alginate stabilized semiconductor nanoparticles, Bull Korean Chem Soc 33 (10) (Oct. 2012) 3218–3224, https://doi.org/10.5012/bkcs.2012.33.10.3218.

[38] M.Z. Ahmad, A.H. Bin Sabri, Q.K. Anjani, J. Domínguez-Robles, N. Abdul Latip, K.A. Hamid, Design and development of levodopa loaded polymeric nanoparticles for intranasal delivery, Pharmaceuticals 15 (3) (Mar. 2022) 370, https://doi.org/10.3390/ph15030370.

[39] M. Ebadi, S. Bullo, K. Buskara, M.Z. Hussein, S. Fakurazi, G. Pastorin, Release of a liver anticancer drug, sorafenib from its PVA/LDH- and PEG/LDH-coated iron oxide nanoparticles for drug delivery applications, Sci. Rep. 10 (1) (Dec. 2020) 21521, https://doi.org/10.1038/s41598-020-76504-5.

[40] N. Ngwuluka, N. Ochekpe, O. Aruoma, Naturapolyceutics: the science of utilizing natural polymers for drug delivery, Polymers 6 (5) (May 2014) 1312–1332, https://doi.org/10.3390/polym6051312.

[41] A. Salisu, M.M. Sanagi, A. Abu Naim, K.J. Abd Karim, W.A. Wan Ibrahim, U. Abdulganiyu, Alginate graft polyacrylonitrile beads for the removal of lead from aqueous solutions, Polym. Bull. 73 (2) (Feb. 2016) 519–537, https://doi.org/10.1007/s00289-015-1504-3.

[42] R.B. Lima, R. Raza, H. Qin, J. Li, M.E. Lindström, B. Zhu, Direct lignin fuel cell for power generation, RSC Adv. 3 (15) (2013) 5083, https://doi.org/10.1039/c3ra23418e.

[43] M.E. Neto, et al., Synthesis and characterization of zinc, iron, copper, and manganese oxides nanoparticles for possible application as plant fertilizers, J. Nanomater. 2023 (Feb. 2023) 1–8, https://doi.org/10.1155/2023/1312288.